Acta Pharmaceutica Sinica B 2024;14(1):421−432

Chinese Pharmaceutical Association
Institute of Materia Medica, Chinese Academy of Medical Sciences

Acta Pharmaceutica Sinica B

www.elsevier.com/locate/apsb
www.sciencedirect.com

ORIGINAL ARTICLE

Genomics-driven derivatization of the bioactive fungal sesterterpenoid variecolin: Creation of an unnatural analogue with improved anticancer properties

Dexiu Yan[a,b,†], Jemma Arakelyan[a,b,†], Teng Wan[a,b], Ritvik Raina[b,c], Tsz Ki Chan[a,b], Dohyun Ahn[a,b], Vladimir Kushnarev[a], Tsz Kiu Cheung[a,b], Ho Ching Chan[a,b], Inseo Choi[a,b], Pui Yi Ho[a,b], Feijun Hu[a,b], Yujeong Kim[a,b], Hill Lam Lau[a,b], Ying Lo Law[a,b], Chi Seng Leung[a,b], Chun Yin Tong[a,b], Kai Kap Wong[a,b], Wing Lam Yim[a,b], Nikolay S. Karnaukhov[d], Richard Y.C. Kong[a,b,*], Maria V. Babak[a,b,*], Yudai Matsuda[a,b,*]

[a]*Department of Chemistry, City University of Hong Kong, Hong Kong SAR, China*
[b]*iGEM Team "VarieCure", City University of Hong Kong, Hong Kong SAR, China*
[c]*Department of Biomedical Engineering, City University of Hong Kong, Hong Kong SAR, China*
[d]*Moscow Clinical Research Center Named After A.S. Loginov, Moscow 111123, Russian Federation*

Received 24 May 2023; received in revised form 25 July 2023; accepted 24 August 2023

KEY WORDS

Animal studies;
Anticancer properties;
Biosynthesis;
Natural products;
Sesterterpenoids;

Abstract A biosynthetic gene cluster for the bioactive fungal sesterterpenoids variecolin (**1**) and variecolactone (**2**) was identified in *Aspergillus aculeatus* ATCC 16872. Heterologous production of **1** and **2** was achieved in *Aspergillus oryzae* by expressing the sesterterpene synthase VrcA and the cytochrome P450 VrcB. Intriguingly, the replacement of VrcB with homologous P450s from other fungal terpenoid pathways yielded three new variecolin analogues (**5**−**7**). Analysis of the compounds' anticancer activity *in vitro* and *in vivo* revealed that although **5** and **1** had comparable activities, **5** was associated with significantly reduced toxic side effects in cancer-bearing mice, indicating its potentially broader therapeutic

*Corresponding authors.
E-mail addresses: bhrkong@cityu.edu.hk (Richard Y.C. Kong), mbabak@cityu.edu.hk (Maria V. Babak), ymatsuda@cityu.edu.hk (Yudai Matsuda).
[†]These authors made equal contributions to this work.
Peer review under the responsibility of Chinese Pharmaceutical Association and Institute of Materia Medica, Chinese Academy of Medical Sciences.

https://doi.org/10.1016/j.apsb.2023.08.025

Synthetic biology;
Terpene synthases;
Variecolin

window. Our study describes the first tests of variecolin and its analogues in animals and demonstrates the utility of synthetic biology for creating molecules with improved biological activities.

1. Introduction

Sesterterpenoids are a class of terpenoids derived from five isoprene (C_5) molecules and are widely distributed in nature but relatively rare compared with other terpenoid species[1−3]. Fungi are prolific producers of sesterterpenoids with a wide range of biological activities, such as ophiobolin A, which exerts potent anticancer activity[4]. Since the discovery and characterization of the first sesterterpene synthase in 2013[5], the biosynthetic pathways of several fungal sesterterpenoids have been elucidated[6−9]. Several new sesterterpenoids have been obtained using a genome mining approach that targets unexploited fungal sesterterpene synthase genes[10−22]. The characterized fungal sesterterpene synthases were found to be chimeric proteins comprising C-terminal prenyltransferase (PT) and N-terminal terpene cyclase (TC) domains. The PT domain is responsible for synthesizing C_{25} geranylfarnesyl pyrophosphate (GFPP), using one molecule of dimethylallyl pyrophosphate (DMAPP) and four molecules of isopentenyl pyrophosphate (IPP) as substrates, whereas the TC domain produces a cyclized product *via* the ionization-initiated (class I) cyclization of GFPP[23]. Finally, this cyclized product is converted into a sesterterpenoid through tailoring reactions. Interestingly, the biosynthetic gene clusters of fungal sesterterpenoids are more compact than those of other fungal secondary metabolites, suggesting that fungal sesterterpenoid biosynthesis may be easily engineered to generate diverse analogues.

Variecolin (**1**) is a tetracyclic sesterterpenoid originally isolated from the fungus *Aspergillus variecolor* MF138 and acts as an angiotensin II receptor binding inhibitor[24]. Subsequently, **1** and its congeners such as variecolactone (**2**) and emericolin A (**3**) were obtained from several different fungi and have been proven to possess diverse biological activities (Fig. 1A)[25−30], including antifungal[25], immunomodulatory[27], C−C chemokine receptor 5 (CCR5) inhibitory[28], antibacterial[29], antimalarial[30], and anticancer[30] activities. The biological activities and intriguing molecular framework of **1** have inspired synthetic chemists to attempt the synthesis of this sesterterpenoid[31−34]; however, **1** is a challenging synthetic target, and its total synthesis has not been achieved. Furthermore, despite recent rapid advances in biosynthetic studies on fungal sesterterpenoids, the biosynthetic genes for **1** have not been reported. Thus, identification and characterization of the biosynthetic gene cluster for **1** would facilitate the efficient production and structural modification of this medicinally important molecule *via* biocatalytic or synthetic biological approaches.

In this study, to achieve the heterologous biosynthesis and derivatization of **1**, we first identified the biosynthetic gene cluster for **1** in *Aspergillus aculeatus*. Then, we heterologously produced **1** using the terpene synthase VrcA and the cytochrome P450 monooxygenase VrcB. We also used a series of VrcB homologues to obtain three new variecolin analogues. Finally, we evaluated the biological activity of the obtained molecules in a mouse model and found that one of the newly synthesized variecolin analogues exerted promising anticancer activity with significantly less toxicity than **1**.

2. Results and discussion

2.1. Discovery of the biosynthetic gene cluster of variecolin in *Aspergillus aculeatus*

To discover the biosynthetic gene cluster of **1**, we examined the sequence of the *A. aculeatus* ATCC 16872 (CBS 172.66) genome[35], as *A. aculeatus* is a known producer of **1**[30]. This investigation revealed the presence of two homologous proteins of known sesterterpene synthases. As the molecular backbone of **1** is expected to be biosynthesized in a similar manner as that of astellifadiene[11], the terpene synthase required for variecolin biosynthesis should display high sequence identity with astellifadiene synthase (EvAS). One possible sesterterpene synthase in *A. aculeatus* was found to exhibit 65% amino acid sequence identity with EvAS, and we therefore reasoned that this enzyme may be involved in the biosynthesis of **1**. In the flanking region of this terpene synthase gene, we observed genes encoding a cytochrome P450 monooxygenase and an ATP-binding cassette (ABC) transporter, which appeared to form a cluster with the terpene synthase gene (Fig. 1B). This gene cluster (hereafter, *vrc* cluster) is conserved among several fungi, including the known variecolin producer *Aspergillus japonicus*[36], further supporting its involvement in the biosynthesis of **1**. Based on this gene cluster information, the following route of variecolin biosynthesis was predicted: the sesterterpene synthase VrcA first yields a hydrocarbon with the backbone of **1**, which then undergoes multiple oxidations catalyzed by the P450 VrcB to yield **1** (Fig. 1C).

2.2. Elucidation of the variecolin biosynthesis

To analyze the function of the *vrc* cluster, we heterologously expressed the terpene synthase gene *vrcA* in *Aspergillus oryzae* NSAR1[37], a powerful platform for the heterologous reconstitution of fungal metabolite biosynthesis[38−43]. The metabolites derived from this *A. oryzae* transformant were analyzed by GC−MS. A new compound **4** with an *m/z* of 340 $[M]^+$, which corresponds to a sesterterpene hydrocarbon, was detected only in the transformant harboring *vrcA* (Fig. 2A). After large-scale cultivation of the transformant, **4** was isolated and subjected to MS and NMR analysis for structural characterization. HR-APCI-MS analysis showed the molecular formula of **4** was $C_{25}H_{40}$, with six degrees of unsaturation. Four olefinic carbon signals were observed in the ^{13}C NMR spectrum of **4**, indicating the tetracyclic nature of the

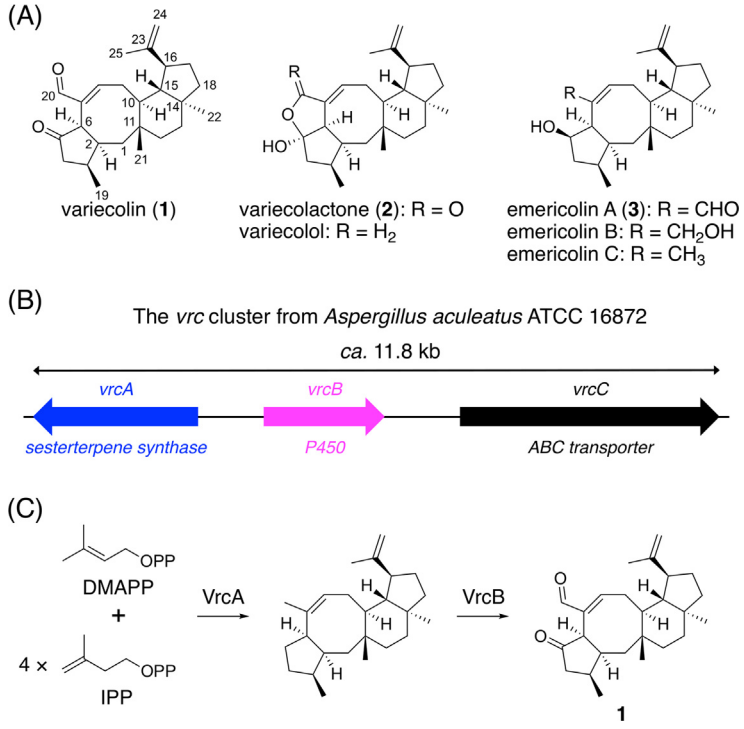

Figure 1 (A) Structures of variecolin (**1**) and its selected analogues. (B) Schematic representation of the *vrc* cluster. (C) Predicted biosynthetic pathway of **1**.

product. Further analysis of the 2D NMR spectra revealed that **4** possesses a carbon skeleton identical to that of **1** (Supporting Information Fig. S1) and therefore is likely to be the biosynthetic precursor of **1**. Compound **4** was named variecoladiene (Fig. 2C).

The cyclization of GFPP to form **4** should occur in a manner resembling that of astellifadiene (Fig. 3), as previously discussed[11]. Thus, after the departure of the pyrophosphate group, C−C bonds form at C-1/C-11 and C-10/C-14 to generate the bicyclic intermediate $\mathbf{4a}^+$ with an 11-5-fused ring system. Next, the five-membered ring undergoes ring expansion, concomitant with the formation of an additional ring at C-14/C-18. The resultant 11-6-5-fused tricyclic cation $\mathbf{4b}^+$ is then neutralized by deprotonation from C-24 to yield **4c**. Subsequently, C-3 is reprotonated, followed by the formation of a C−C bond at C-2/C-6 to provide $\mathbf{4d}^+$ with a 5-8-6-5-fused ring system. This reprotonation was experimentally confirmed in an EvAS-catalyzed reaction[11]. Finally, deprotonation from C-8 installs a double bond between C-7 and C-8 to complete the cyclization reaction.

We then co-expressed the P450 gene *vrcB* along with the terpene synthase gene *vrcA* in *A. oryzae*, and consequently, two major peaks were observed in the HPLC analysis of the metabolites produced by the two gene-expressing strains (Fig. 2B, trace iii). The major products **1** and **2** were then purified and identified as variecolin and variecolactone, respectively, by the comparison of their NMR spectra and specific rotation values with the literature data[26,27]. This also allowed the determination of the absolute configuration of **4**, as shown in Fig. 2C. In the course of the purification procedure, we noticed the presence of another minor metabolite, which was also isolated and identified as emericolin A (**3**)[28]. Thus, it is indicated that the P450 VrcB is solely responsible for the multiple oxidations at C-5 and C-20 positions; similar multifunctional P450s have been found in several sesterterpenoid biosynthetic pathways[6–8,10,12,15]. Collectively, it has been proven that the *vrc* cluster is indeed responsible for the variecolin biosynthesis, and heterologous production of **1** was successfully achieved.

2.3. *Creation of unnatural sesterterpenoid pathways*

Having established a heterologous platform for variecolin (**1**) production, we next sought to derivatize the scaffold of **1** using the *A. oryzae* system. To this end, we collected known P450 genes involved in fungal di-/sesterterpenoid biosynthesis and uncharacterized P450 genes found to be clustered with potential di-/sesterterpene synthase genes; we sought to include diverse P450s, ranging from close homologues of VrcB to those exhibiting little similarity with VrcB (Supporting Information Table S2 and Figs. S2 and S3). These collected P450 genes were then utilized as genetic building blocks to construct artificial sesterterpenoid pathways. Each P450 gene was individually co-expressed with the sesterterpene synthase gene *vrcA*; four of the 17 tested P450s yielded oxidized products of **4**. Two P450s from *Aspergillus violaceofuscus* CBS 115571[44] (designated as VrcB'; GenBank: PYI14930.1) and *Aspergillus heteromorphus* CBS 117.55[44] (designated as VrcB"; GenBank: XP_025395330.1) exhibited the same product profile as VrcB (Fig. 2B, trace iv and v). This is consistent with the high sequence similarity between VrcB and the two P450s (89% and 79% amino acid identity, respectively). Intriguingly, the introduction of *acldA-P450*, which is involved in the biosynthesis of asperterpenol B[9], afforded a new metabolite, **5** (Fig. 2B, trace vi), which was revealed to be a monooxygenated form of **4** by HR-MS analysis. Further analysis of the NMR spectra confirmed that **5** harbors a hydroxy group at C-4. The stereochemistry at C-4 was deduced based on the NOESY correlation between H-4 and H_3-19 (Fig. 2C and Fig. S1), and was further confirmed using the modified Mosher's method

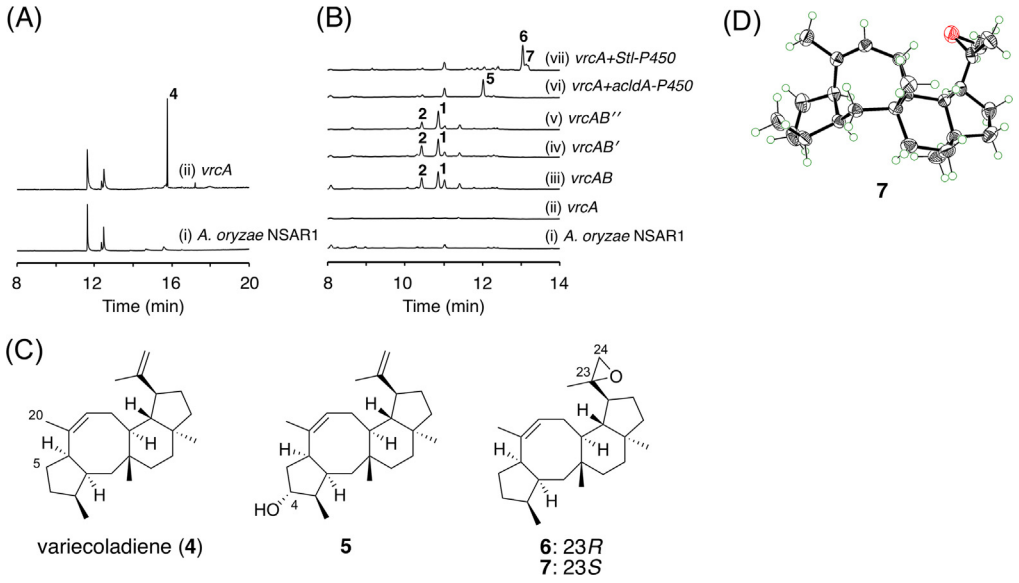

Figure 2 (A) GC−MS chromatograms of *A. oryzae* transformants. (B) HPLC chromatograms of the *A. oryzae* transformants. The chromatograms were monitored at 215 nm. (C) Structures of the metabolites obtained in this study. (D) X-ray crystal structure of **7**.

(Supporting Information Fig. S4)[45]. This observation is consistent with the fact that AcldA-P450 performs the C-4α hydroxylation on its native substrate[9]. Compound **5** was hereby named 4α-hydroxyvariecoladiene. Moreover, Stl-P450, which is responsible for stellatic acid biosynthesis[6], transformed **4** into two products, **6** and **7** (Fig. 2B, trace vii), both of which were isomers of **5**. The NMR spectra of **6** and **7** were very similar and lacked exo-methylene signals at C-23/C-24. Two doublets at 2.5−2.7 ppm in the ^{1}H NMR spectra of **6** and **7** were not observed in the ^{1}H NMR spectrum of **4**; likewise, there were two new signals at 55−61 ppm in the ^{13}C NMR spectra of **6** and **7**, implying that the exo-methylene was epoxidized by Stl-P450. Analysis of the 2D NMR spectra of **6** and **7** confirmed that they had the same planar structure, with an epoxide at C-23/C-24, and only differed in the stereochemistry at C-23 (Fig. 2C and Fig. S1). Fortunately, **7** was crystallized and subjected to X-ray diffraction analysis, which, along with the absolute configuration of **1**, determined the stereochemistry of the epoxide in **7** to be *S* (Fig. 2D; CCDC: 2217442). Accordingly, it was deduced that **6** has the 23*R* configuration. Compounds **6** and **7** were designated as (23*R*)- and

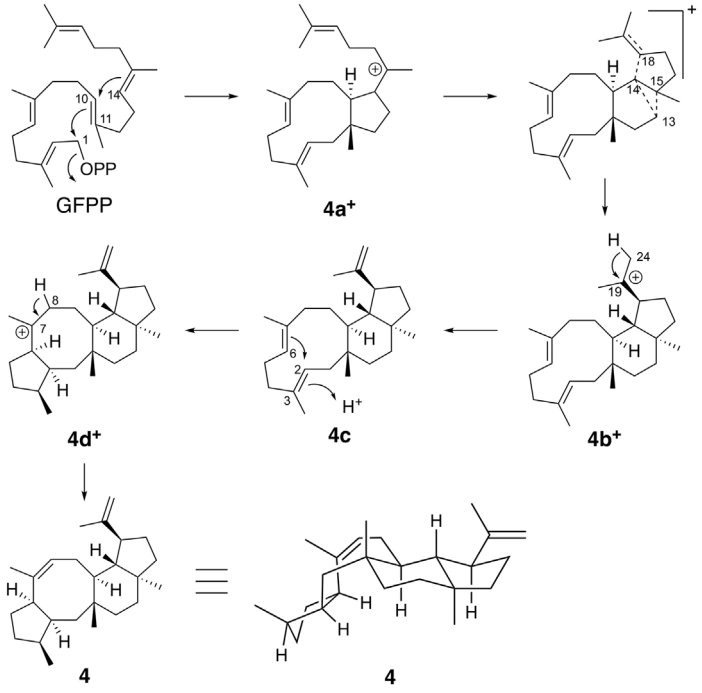

Figure 3 Proposed mechanism of the VrcA-catalyzed cyclization. The carbon atom numbering is in accordance with that for the EvAS-catalyzed reaction.

(23*S*)-oxidovariecoladiene, respectively. Interestingly, Stl-P450 oxidizes a methyl group to a carboxy group in stellatic acid biosynthesis (Fig. S3), which is distinct from the reaction that occurred on the variecolin scaffold.

2.4. *Investigation of the anticancer activity of variecolin and its analogues*

All of the compounds except **3** were obtained in sufficient quantities and purities for biological testing (Supporting Information Fig. S5), and therefore, we evaluated their biological activities. As the compounds were poorly soluble in water, stock solutions were prepared in DMSO and subsequently diluted with complete Dulbecco's Modified Eagle Medium (DMEM) cell-culture media. The stability of compounds **1**, **2**, and **4**−**7** in DMSO was assessed using ^{1}H NMR spectroscopy at 0, 24, 48, and 72 h, and all of the compounds were found to be stable throughout the experimental period (Supporting Information Fig. S6). We then assessed the cytotoxicity of **1**, **2**, and **4**−**7** in the human breast adenocarcinoma cell line MCF-7 and murine colon cancer cell line CT26 using a colorimetric MTT assay with an exposure time of 72 h (Table 1 and Supporting Information Fig. S7). All of the tested compounds demonstrated activity at low to high micromolar concentrations in both cancer cell lines with the exception of **4**, which was not cytotoxic in MCF-7 cells. The cytotoxicities of **1** and **2** were previously assessed in MCF-7 cells (IC_{50} = 30.99 and 14.47 μmol/L, respectively); however, those data cannot be directly compared with the data from the current study because the incubation time and standard deviations were not reported[30]. Our results indicate that the anticancer activities of the compounds increased in the following order: **4** ≪ **6** < **7** < **2** < **5** < **1**. The comparison of **4** and **6** revealed a significant difference in their cytotoxicities (4.3 and 6.8-times in MCF-7 and CT26 cells, respectively), demonstrating that epoxidation at C-23/C-24 significantly improved the anticancer activity of this scaffold compound. Although **6** and **7** only differed in terms of their stereochemistry at C-23, the cytotoxicity of **7** was 3.9 and 3.2-times higher than that of **6** in MCF-7 and CT26 cells, respectively. The most drastic change in cytotoxicity was revealed by comparing **4** with its hydroxylated form, **5**. The presence of the C-4 hydroxy group on **5** resulted in 63- and 132-fold increases in cytotoxicity in MCF-7 and CT26 cells, respectively. Among all of the tested compounds, **1** and **5** were the most active in both cell lines (IC_{50}s ≈ 1−8 μmol/L). The selectivity of each tested compound toward cancer cells is represented by a selectivity factor (SF), which was calculated as the ratio of the IC_{50} value in the non-cancerous human lung fibroblast cell line (MRC-5) to that in the respective cancer cell line. All of the compounds except **5** were as toxic in MRC-5 cells (SF ≤ 1) as in cancer cells (Table 1), or more toxic in MRC-5 cells than in cancer cells, suggesting they may cause serious side effects during treatment. Similarly, poor selectivity is typically observed for anticancer natural product drugs such as paclitaxel and doxorubicin[46,47]. That is, despite being very effective, these drugs can cause severe toxicity in cancer patients, including heart toxicity and peripheral neuropathy[48,49]. In contrast, compared with **1**, the unnatural analogue **5** was less cytotoxic but was selective for cancer cells over normal cells (SF ≈ 1.4−3.5), indicating that this compound may potentially offer a wider therapeutic window, more flexible dosing, and fewer adverse effects.

2.5. *In vivo evaluation of antitumor efficacy of variecolin (**1**) and **5** in mouse colon cancer xenograft model*

Variecolin (**1**) and **5** were chosen for subsequent *in vivo* studies. To determine the appropriate dose, we conducted a pilot acute toxicity study in BALB/c mice. The mice (n = 15) were randomly distributed into five groups and intraperitoneally injected every other day with **1** or **5** or vehicle (five injections within 10 days). The groups received the following treatments: Group 1, 10 mg/kg of **1**; Group 2, 20 mg/kg of **1**; Group 3, 10 mg/kg of **5**; Group 4, 20 mg/kg of **5**; and Group 5, vehicle. The mice were monitored daily to detect weight changes and clinical signs of toxicity. After the last injection, the animals were followed for seven days to watch for signs of delayed toxicity. Mice in Groups 3−5 did not exhibit any signs of toxicity during the observation period. In contrast, all of the mice in Group 2, which received the highest dose of **1**, died spontaneously after the second injection (Day 4). Initially, the mice in Group 1 tolerated treatment with a low dose of **1**, as indicated by a lack of weight loss or other signs of toxicity. However, during the follow-up period, all of these mice started to show signs of toxicity, such as severe diarrhea and weight loss, so were humanely sacrificed. These *in vivo* results are consistent with those of the *in vitro* selectivity study described above. Therefore,

Table 1 Anticancer activity of the metabolites **1**, **2**, and **4**−**7**.

Compd.	IC_{50} (μmol/L)[a]			SF_{MCF-7}[b]	SF_{CT26}[c]
	MCF-7	CT26	MRC-5		
Variecolin (**1**)	1.4 ± 0.3	1.0 ± 0.3	1.1 ± 0.2	0.8	1.1
Variecolactone (**2**)	22 ± 8	14 ± 3	15 ± 3	0.7	1.1
Variecoladiene (**4**)	>500	409 ± 131	>500	−	−
5	8 ± 2	3.1 ± 0.5	11 ± 3	1.4	3.5
6	117 ± 29	60 ± 10	33 ± 6	0.3	0.5
7	30 ± 8	19 ± 7	14 ± 5	0.5	0.7
Paclitaxel[d]	0.00278	n.d.[e]	0.00261	0.9	−

[a]Half-maximal (50%) inhibitory concentrations in the MCF-7 (human breast adenocarcinoma) and CT26 (murine colon carcinoma) cell lines, as determined using an MTT assay with an exposure time of 72 h. Values are means ± standard deviations obtained from at least three independent experiments.

[b]The selectivity factor (SF) was calculated as IC_{50}(MRC-5)/IC_{50}(MCF-7).

[c]The SF was calculated as IC_{50}(MRC-5)/IC_{50}(CT26).

[d]The IC_{50} values and SF_{MCF-7} were taken from the literature[45].

[e]n.d. = not determined.

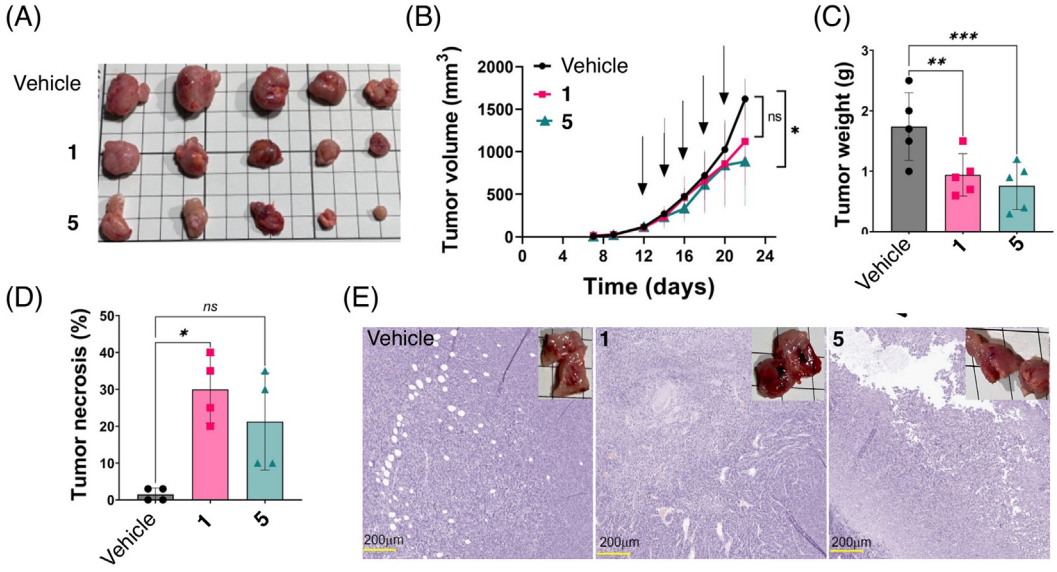

Figure 4 Effects of **1** and **5** on CT26 tumor growth *in vivo*. (A) Representative images of tumors at the study endpoint after five intraperitoneal (i.p.) injections of **1**, **5**, or vehicle (DMSO/Cremophor EL in sterile PBS). (B) CT26 tumor growth over time in BALB/c mice. The tumors first became palpable on Day 7, and their volumes were measured with calipers every other day. Mice ($n = 5$) were treated with **1** at 8 mg/kg, **5** at 20 mg/kg, or vehicle *via* i.p. injection every other day (arrows represent the injection days). (C) Weights of the isolated tumors shown in Fig. 4A. (D) Quantification of necrosis in hematoxylin- and eosin-(H&E) stained tumor tissues. (E) Representative H&E-stained tumor tissues from vehicle, **1**, and **5**-treated mice. (B) Two-way analysis of variance with Dunnett's *post-hoc* analysis or (C and D) unpaired *t*-tests were conducted using GraphPad Prism 9 software (GraphPad Software Inc., La Jolla, CA, USA); $P < 0.05$ is considered significant ($^*P < 0.05$, $^{**}P < 0.01$, $^{***}P < 0.001$, ns: not significant).

we chose subtoxic dosage of 8 mg/kg of **1** and 20 mg/kg of **5** for subsequent efficacy studies.

Next, we established a mouse xenograft model using the colorectal cancer cell line CT26. The animals ($n = 15$) were randomly divided into three groups and treated as follows: Group 1, **1** (8 mg/kg); Group 2, **5** (20 mg/kg); and Group 3, vehicle (1% DMSO/Cremophor EL in sterile phosphate-buffered saline [PBS]). Cremophor EL was used to ensure sufficient solubility of the tested compounds in aqueous buffers. As soon as the tumors became palpable (Day 7), their volumes were measured every other day. On Day 12, the mice were intraperitoneally injected with the indicated compound or vehicle every second day for 10 consecutive days (a total of five injections). Throughout the experiment, all of the mice remained bright, alert, and responsive and did not exhibit any clinical signs of toxicity (no body weight changes exceeding 5%, and no diarrhea; Supporting Information Fig. S8). When the tumor volume in the control group reached 2000 mm^3, all animals were humanely sacrificed, and the tumors, kidneys, and livers were harvested for further histological examination. The kidneys and livers from all three groups demonstrated a normal structure without significant microscopic structural changes (Supporting Information Fig. S9). Analysis of the tumor volumes at the experimental endpoint revealed that mice treated with **5**, but not those treated with **1**, demonstrated significant inhibition of tumor growth (Fig. 4A and B). However, the tumor weights were significantly reduced in both treatment groups relative to the controls (Fig. 4C). The histological examination of tumor tissues from drug-treated mice revealed high levels of necrosis, especially in the group treated with **1** (Fig. 4D and E). In contrast, tumors from the vehicle-treated group exhibited rapid growth and low levels of necrosis. In conclusion, both **1** and **5** were able to reduce the tumor burden; however, the efficacy of **1** was markedly limited by its toxicity, whereas **5** was not toxic, even at the highest dose (20 mg/kg). To the best of our knowledge, this is the first study to explore the *in vivo* antitumor efficacy of **1** and its analogues.

3. Conclusions

In this study, we successfully achieved the heterologous production of variecolin (**1**), which has long been a challenging target for synthetic chemists. Furthermore, we derivatized the scaffold of **1** by employing P450s from other fungal terpenoid pathways, and thus obtained three distinct biocatalysts that can efficiently oxidize the skeleton of **1**. Given that the new analogues of **1** with different oxidative modifications all exhibited anticancer activity, the skeleton of **1** could be considered a privileged scaffold for developing anticancer agents. Most significantly, one of its derivatives, **5**, was characterized by a wider therapeutic window with an ideal combination of toxicity and efficacy, which is in clear contrast to **1** exhibiting higher cytotoxicity but severer side effects. Given the structural differences between **1** and **5**, the aldehyde group of **1**, which would react with various biological molecules, might be attributed to the toxic side effects of **1**. Although many additional investigations have yet to be performed for further application of **5**, these findings demonstrate the utility of our synthetic biology strategy to obtain bioactive unnatural natural products. This approach could also be applied to the structural modification of other fungal sesterterpenoids, which would further diversify this class of natural products and possibly provide future lead compounds with improved biological activities.

4. Experimental

4.1. General experimental procedures

Organic solvents were purchased from Anaqua (Hong Kong) Co. Ltd., and other chemicals were purchased from Wako Chemicals Ltd., Thermo Fisher Scientific, Sigma−Aldrich, or J&K Scientific Ltd., unless noted otherwise. Oligonucleotide primers (Supporting Information Table S4) were purchased from Tech Dragon Limited or Beijing Genomics Institute. Thiazolyl blue tetrazolium bromide (MTT) was purchased from Alfa Aesar, Roswell Park Memorial Institute (RPMI 1640) medium, Dulbecco's Modified Eagle's Medium (DMEM) medium, Fetal Bovine Serum (FBS), Phosphate Buffered Saline (PBS), Tris-acetate EDTA were purchased from Thermo Fisher Scientific. Milli-Q-grade purified water was obtained from a Milli-Q UV purification system (Sartorius Stedim Biotech S.A., Aubagne Cedex, France). 2′,7′-Dichlorodihydrofluorescein diacetate and Cremophor EL were purchased from Sigma−Aldrich. PCR was performed using a T100 Thermal Cycler (Bio-Rad Laboratories, Inc.) with Phanta Max Super-Fidelity DNA Polymerase (Vazyme Biotech Co., Ltd.). Analytical HPLC was performed on a Dionex Ultimate 3000 UHPLC system (Thermo Scientific), using a Kinetex 2.6 μm C_{18} 100 Å column (2.1 mm i.d. × 100 mm; Phenomenex). Preparative HPLC was performed on a Waters 1525 Binary HPLC pump with a 2998 photodiode array detector (Waters Corporation), using a an XBridge BEH C18 OBD Prep Column (100 Å, 5 μm, 19 mm i.d. × 250 mm; Waters Corporation). Flash chromatography was performed using an Isolera Spektra One flash purification system (Biotage). NMR spectra were obtained at 600 MHz (^{1}H)/150 MHz (^{13}C) with a Bruker Ascend Avance III HD spectrometer, and chemical shifts were recorded with reference to solvent signals (^{1}H NMR: $CDCl_3$ 7.26 ppm; ^{13}C NMR: $CDCl_3$ 77.0 ppm). HR-ESI-MS and HR-APCI-MS spectra were obtained with a SCIEX X500R Q-TOF mass spectrometer. Optical rotations were measured with P-2000 Digital Polarimeter (JASCO Corporation). GC−MS analyses were performed with an Agilent 7890A/5975C system using an HP-5ms capillary column (0.25 mm i.d. × 30 mm, 0.25 μm film thickness).

4.2. Strains

Emericella variecolor NBRC 32302 was obtained from the Biological Resource Center, National Institute of Technology and Evaluation (Chiba, Japan), and the other fungal strains listed in Table S2 were purchased from the Westerdijk Fungal Biodiversity Institute. *A. oryzae* NSAR1 (*niaD*$^-$, *sC*$^-$, *ΔargB*, *adeA*$^-$)[37] was utilized as the fungal heterologous expression host. Standard DNA engineering was performed with *Escherichia coli* DH5α (Takara Bio Inc.).

4.3. Construction of fungal transformation plasmids

To construct the fungal transformation plasmid with *vrcA*, it was first amplified from the genomic DNA of *E. variecolor* NBRC 32302 and introduced into pTAex3 vector[50], using a ClonExpress Ultra One Step Cloning Kit (Vazyme Biotech Co., Ltd.). A DNA fragment harboring the *amyB* promoter (*PamyB*)-*vrcA*-*amyB* terminator (*TamyB*) was then amplified from the pTAex3-based plasmid, and further introduced into the pAdeA vector[51]. Meanwhile, each P450 gene was amplified from the genomic DNA of the corresponding fungal strain and ligated into the pTAex3-HR vector[52]. Primers used in this study and detailed methods for the construction of the plasmids are summarized in Supporting Information Tables S4 and S5, respectively.

4.4. Fungal transformation

Initially, *A. oryzae* NSAR1 was transformed with pAdeA-vrcA by the previously reported protoplast−polyethylene glycol method[53]. Subsequently, the resultant transformant was further transformed using the pTAex3-HR-based plasmid containing each P450 gene by CRISPR-Cas9-mediated DNA double-strand break and repair by homologous recombination, as previously described[52]. Transformants created in this study and the plasmids used for the transformation are given in Supporting Information Table S6.

4.5. GC−MS and HPLC analysis of each product from *A. oryzae* transformants

To analyze the metabolites from each *A. oryzae* transformant, the transformants were cultivated on a DPY agar plate [2% dextrin, 1% hipolypepton (Nihon Pharmaceutical Co., Ltd.), 0.5% yeast extract, 0.5% KH_2PO_4, 0.05% $MgSO_4 \cdot 7H_2O$, and 1.5% agar] for seven days at 30 °C. A small piece of fungal mycelia and agar was cut from the plate, soaked in ethyl acetate, and extracted using an ultrasonic bath. The ethyl acetate layer was transferred to a new tube, and the solvent was removed using nitrogen gas flow.

For the analysis of the metabolites from the *A. oryzae* transformant harboring *vrcA*, the extract was subjected to a GC−MS analysis. The temperature of the ionization chamber was 260 °C, with electron impact ionization at 70 eV. Helium was used as a carrier gas, and its average velocity was 27.573 cm/s. The program held the temperature at 100 °C for 3 min, increased the temperature at a rate of 14 °C/min up to 268 °C, and then held it at 268 °C for 6 min.

HPLC analyses were performed with a solvent system of 20 mmol/L formic acid (solvent A) and acetonitrile containing 20 mmol/L formic acid (solvent B), at a flow rate of 0.4 mL/min and a column temperature of 40 °C. Separation was performed using a linear gradient from 10:90 (solvent B/solvent A) to 100:0 for 10 min, 100:0 for the following 3 min, and a linear gradient from 100:0 to 10:90 within the following 2.0 min, and then 10:90 for 2.5 min of equilibrium.

4.6. Isolation of each metabolite

To isolate each metabolite, *A. oryzae* transformants were cultivated on DPY agar plates at 30 °C for seven days. Then fungal cultures and agar medium were crushed into small pieces, soaked in ethyl acetate, and extracted twice using an ultrasonic bath. After filtration, ethyl acetate was removed *in vacuo*. The crude extract was fractionated by flash chromatography or silica-gel column chromatography, and further purified by preparative HPLC. Purification methods for each compound are described in detail below.

4.6.1. Purification conditions for variecolin (**1**), variecolactone (**2**), and emericolin A (**3**)

A. oryzae NSAR1 with *vrcA* and *vrcB* was cultivated on 150 DPY agar plates (*ca.* 3 L) at 30 °C for seven days. The extract from the transformant (1.64 g) was subjected to flash chromatography and

eluted stepwise using a dichloromethane:ethyl acetate gradient (100:0 to 0:100). Fractions that contained **1** were then purified by reverse-phase preparative HPLC (90% aqueous acetonitrile, 10.0 mL/min) to yield 31.7 mg of white powder. Fractions that contained **2** were purified by reverse-phase preparative HPLC (90% aqueous acetonitrile, 10.0 mL/min) to yield 63.5 mg of white powder. Fractions that contained **3** were purified by reverse-phase preparative HPLC (80% aqueous acetonitrile, 10.0 mL/min) to yield 4.7 mg of white powder.

4.6.2. *Purification conditions for variecoladiene (**4**)*

A. oryzae NSAR1 with *vrcA* was cultivated on 50 DPY agar plates (*ca.* 1 L) at 30 °C for seven days. The extract from the transformant (432 mg) was reextracted with hexane and then subjected to silica-gel column chromatography and eluted with hexane to finally yield 13.0 mg of colorless oil.

4.6.3. *Purification conditions for compound **5***

A. oryzae NSAR1 with *acldA-P450* was cultivated on 150 DPY agar plates (*ca.* 3 L) at 30 °C for seven days. The extract from the transformant (820 mg) was subjected to silica-gel column chromatography and eluted with hexane: ethyl acetate (100:0−10:1). Fractions that contained **5** were then purified by reverse-phase preparative HPLC (95% aqueous acetonitrile, 10.0 mL/min) to yield 14.3 mg of colorless oil.

4.6.4. *Purification conditions for compounds **6** and **7***

A. oryzae NSAR1 with *Stl-P450* was cultivated on 150 DPY agar plates (*ca.* 3 L) at 30 °C for seven days. The extract from the transformant (750 mg) was subjected to silica-gel column chromatography and eluted with hexane: ethyl acetate (100:0−99:1). Fractions that contained **6** and **7** were then purified by reverse-phase preparative HPLC (95% aqueous acetonitrile, 10.0 mL/min) to yield 18.2 mg of colorless oil (**6**) and 6.2 mg of colorless oil (**7**).

4.7. *Synthesis of (S)-MTPA ester of compound **5***

(*R*)-MTPA chloride (82.8 mg) was added to a solution of **5** (5.3 mg) in dry pyridine (1 mL) at room temperature. After 1 h, the reaction mixture was concentrated to dryness and purified by reverse-phase preparative HPLC (98% acetonitrile) to yield 6.8 mg of (*S*)-MTPA ester of **5**. ^{1}H NMR ($CDCl_3$, 600 MHz): δ 5.55 (1H, brd, J = 7.2 Hz, H-8), 5.19 (1H, d, J = 4.8 Hz, H-4), 4.68 (1H, d, J = 1.9 Hz, H-24), 4.56 (1H, brs, H-24), 3.41 (1H, q, J = 9.4 Hz, H-6), 2.55 (1H, td, J = 11.1, 7.2 Hz, H-2), 2.39 (1H, td, J = 10.8, 5.1 Hz, H-16), 2.34 (1H, brd, J = 17.6 Hz, H-9α), 2.27 (1H, ddd, J = 15.4, 7.5, 5.3 Hz, H-5β), 2.09 (1H, quin, J = 7.2 Hz, H-3), 2.04 (1H, overlapped, H-10), 2.00 (1H, m, H-5α), 1.94 (1H, m, H-17α), 1.69 (3H, s, H-25), 1.65 (1H, m, H-1β), 1.65 (3H, s, H-20), 1.65 (1H, overlapped, H-9β), 1.61 (1H, overlapped, H-12α), 1.38 (1H, ddd, J = 12.7, 4.5, 2.5 Hz, H-13α), 1.36 (1H, overlapped, H-18α), 1.33 (1H, overlapped, H-13β), 1.32 (1H, m, H-17β), 1.28 (1H, t, J = 11.1 Hz, H-15), 1.15 (1H, q, J = 10.5 Hz, H-18β), 0.96 (1H, d, J = 13.9 Hz, H-1α), 0.88 (1H, overlapped, H-12β), 0.87 (3H, s, H-21), 0.75 (3H, d, J = 7.4 Hz, H-19), 0.66 (3H, s, H-22); for NMR spectra see Supporting Information Fig. S28.

4.8. *Synthesis of (R)-MTPA ester of compound **5***

The synthesis of the (*R*)-MTPA ester of **5** was performed in the same manner as described for the (*S*)-MTPA ester with **5** (5.4 mg) and (*S*)-MTPA chloride (84.3 mg), yielding 7.8 mg of (*R*)-MTPA ester of **5**. ^{1}H NMR ($CDCl_3$, 600 MHz): δ 5.55 (1H, brd, J = 7.4 Hz, H-8), 5.19 (1H, d, J = 4.8 Hz, H-4), 4.69 (1H, d, J = 1.9 Hz, H-24), 4.56 (1H, brs, H-24), 3.36 (1H, q, J = 9.4 Hz, H-6), 2.64 (1H, td, J = 11.3, 7.0 Hz, H-2), 2.39 (1H, td, J = 10.9, 5.1 Hz, H-16), 2.33 (1H, brd, J = 17.3 Hz, H-9α), 2.24 (1H, ddd, J = 15.4, 7.7, 5.0 Hz, H-5β), 2.15 (1H, quin, J = 7.2 Hz, H-3), 2.05 (1H, td, J = 12.0, 5.0 Hz, H-10), 1.95 (1H, m, H-5α), 1.95 (1H, m, H-17α), 1.70 (1H, td, J = 14.0, 4.5 Hz, H-12α), 1.69 (3H, s, H-25), 1.66 (1H, m, H-1β), δ 1.64 (3H, s, H-20), 1.64 (1H, m, H-9β), 1.41 (1H, ddd, J = 12.7, 4.6, 2.5 Hz, H-13α), 1.36 (1H, overlapped, H-18α), 1.35 (1H, overlapped, H-13β), 1.32 (1H, m, H-17β), 1.28 (1H, t, J = 11.1 Hz, H-15), 1.16 (1H, q, J = 11.0 Hz, H-18β), 0.99 (1H, d, J = 14.1 Hz, H-1α), 0.92 (1H, ddd, J = 13.9, 4.6, 2.5 Hz, H-12β), 0.88 (3H, s, H-21), 0.77 (3H, d, J = 7.5 Hz, H-19), 0.70 (3H, s, H-22); for NMR spectra see Supporting Information Fig. S29.

4.9. *Examination of the purity and stability of isolated compounds*

Purified compounds **1**−**3** and **5**−**7** were analyzed by HPLC with the same condition used for the metabolites from *A. oryzae* transformants, whereas compound **4** was analyzed by HPLC using 100% acetonitrile containing 0.05% formic acid as a sole solvent, at a flow rate of 0.4 mL/min and a column temperature of 40 °C (Fig. S5). To check the stability of **1**−**2** and **4**−**7** in DMSO, these compounds were dissolved in DMSO-d_6, and ^{1}H NMR spectra were obtained at different time points (Fig. S6).

4.10. *Cell lines and culture conditions*

MCF-7 (human breast adenocarcinoma), CT26 (murine colorectal carcinoma), and MRC-5 (human lung fibroblasts, non-cancerous) were obtained from the American Type Culture Collection (ATCC). All cell lines were cultured in DMEM containing 10% FBS and 1% of penicillin−streptomycin (10,000 U/mL). Cells were grown in tissue culture flasks (75 and 25 cm^2, SPL Life sciences). All cell lines were grown at 37 °C in a humidified atmosphere of 95% air and 5% CO_2. All drug stock solutions were prepared in DMSO, and the final concentration in the medium did not exceed 1%, at which cell viability was not inhibited.

4.11. *Inhibition of cell viability assay*

The cytotoxicity of the compounds was determined by colorimetric MTT assay. The cells were harvested from culture flasks by trypsinization and seeded into Cellstar 96-well microculture plates at the seeding density of 6000 cells per well (6×10^4 cells/mL). After cells were allowed to resume exponential growth for 24 h, they were exposed to drugs at different concentrations in media for 72 h. The drugs were diluted in complete medium at the desired concentration and added to each well (100 µL) and serially diluted to other wells. After exposure for 72 h, the media was replaced with MTT in media (5 mg/mL, 100 µL) and incubated for additional 45 min. Subsequently, the medium was aspirated, and the purple formazan crystals formed in viable cells were dissolved in DMSO (100 µL). Optical densities were measured at 570 nm using the BioTek H1 Synergy microplate reader. The quantity of viable cells was expressed in terms of treated/control (T/C) values by comparison to untreated control cells, and 50% inhibitory

concentrations (IC_{50}) were calculated from concentration-effect curves by interpolation. Evaluation was based on means from at least three independent experiments, each comprising three replicates per concentration level.

4.12. *In vivo experiments*

All animal procedures were performed under the Guidelines for Care and Use of Laboratory Animals of the City University of Hong Kong and approved by the Animal Ethics Committee of the City University of Hong Kong. All mice were maintained in the laboratory animal research unit (LARU) of the City University of Hong Kong in specific pathogen-free conditions. All mice experiments were performed in compliance with the guidelines and protocols, which were approved by the institutional and local ethics committee of HKSAR, Department of Health. Six to eight-week-old BALB/c mice were purchased from the Laboratory Animal Research Unit (LARU) of the City University of Hong Kong. Animals were randomly assigned to different groups. Prior to assignment to groups, the weight variation of the animals did not exceed 20% of the mean weight. Animals were grouped and housed in solid bottom polycarbonate cages (5 mice per cage) and provided with pelleted food and water ad libitum. Environmental controls for the animal room were set to maintain 22−27 °C, a relative humidity of 55%−75%, a minimum of 10 air changes/h, and a 12 h light/12 h dark cycle. No known contaminants were present in the diet or water at levels that might interfere with this study. To identify the appropriate dose of the experimental drugs for subsequent *in vivo* efficacy study, BALB/c mice were injected every second day *via* i.p. route with 10 or 20 mg/kg of variecolin (**1**) or 10 or 20 mg/kg of **5** for 10 days (5 injections in total). The control group received only the respective vehicle (DMSO/Cremophor EL/PBS). The location of the i.p. injection was the lower left abdominal quadrant. Animals were controlled for distress development. Their weight changes were monitored daily for the whole duration of the experiment. On Day 4, all mice receiving 20 mg/kg of **1** died. Mice receiving 10 mg/kg of **1** experienced severe diarrhea during the follow-up period. Other mice did not show any signs of toxicity. For *in vivo* efficacy study, BALB/c mice were subcutaneously injected with 0.1 mL of CT26 cells (5×10^6 cells/L) on the right flank.

Tumors became palpable on Day 7 after implantation. After the tumor volume reached 100 mm^3, the treatment was initiated (Day 12 after implantation). Animals were randomly divided into three groups ($n = 5$), and tumor dimensions were measured using a caliper. The volume (mm^3) of the tumor was calculated according to Eq. (1):

$$\text{Tumor volume} = (\text{Longest diameter}) \times (\text{Shortest diameter})^2 \times 0.5 \quad (1)$$

Drug-treated groups were intraperitoneally injected with 8 mg/kg of **1** or 20 mg/kg of **5** in sterile PBS with DMSO/Cremophor EL, whereas control group was injected with sterile PBS with DMSO/Cremophor EL as a vehicle. Treatment was performed on Days 12, 14, 16, 18, and 20. After the end of treatment, animals were sacrificed on Day 24. Animals were controlled for distress development. Their weight changes were monitored every day during the whole duration of the experiment. All mice were bright, alert, and responsive during the whole study. After sacrificing mice, tumors were collected, weighed, and harvested, together with organs (liver and kidney), for further histopathological examination.

4.13. *Histopathological examination*

Tumor, liver, and kidney tissues were fixed in 10% buffered formalin overnight and washed twice with PBS. Tissues were then embedded in paraffin. Sections with a thickness of 4 μm were prepared, mounted on slides, and deparaffinized in xylene (twice). Then sections were rehydrated in a graded series of alcohol (2 × 100% alcohol and 2 × 75% alcohol) and distilled water. Later, sections were stained with a haematoxylin solution, rinsed in water, passed through a 70% ethanol solution containing 1% HCl, and rinsed again with tap water. Sections were stained with eosin for 5 min and rinsed with absolute alcohol and xylene for 5 min[54]. The slides were analyzed using Leica DM2700 microscope and Panoramic 250 Flash III (3D Histech, Hungary). Necrosis, hemorrhages, steatosis in hepatocytes, cell shrinking, nuclear enlargement or pyknosis, chromatin condensation, ruptured cell membrane, and apoptotic body were evaluated as potential signs of liver and kidney toxicity[55]. The extent of tumor necrosis was quantified on H&E-stained slides by evaluating the percent of tumor necrotic area by the visual assessment of an experienced pathologist.

4.14. *Analytical data*

*Variecolin (**1**).* White powder; $[\alpha]_D^{22}$ −80.4 (*c* 1.00, CH_3CN); ^1H NMR ($CDCl_3$, 600 MHz): δ 9.18 (s, 1H), 6.92 (m, 1H), 4.73 (brd, J = 2.1 Hz, 1H), 4.63 (brt, J = 1.7 Hz, 1H), 3.57 (d, J = 10.3 Hz, 1H), 2.86 (d, J = 18.6 Hz, 1H), 2.65 (dt, J = 10.7, 6.8 Hz, 1H), 2.52 (ddd, J = 18.7, 8.3, 0.8 Hz, 1H), 2.46−2.36 (m, 3H), 2.24 (ddd, J = 19.1, 12.6, 6.5 Hz, 1H), 2.19 (brt, J = 12.6 Hz, 1H), 1.99 (dtd, J = 13.8, 10.7, 8.5 Hz, 1H), 1.89 (td, J = 13.8, 4.5 Hz, 1H), 1.71 (brs, 3H), 1.55 (dd, J = 14.6, 11.9 Hz, 1H), 1.50 (ddd, J = 12.9, 4.4, 2.5 Hz, 1H), 1.47−1.34 (m, 4H), 1.23 (q, J = 10.6 Hz, 1H), 1.20 (d, J = 14.8 Hz, 1H), 1.02 (ddd, J = 13.9, 3.9, 2.6 Hz, 1H), 0.93 (s, 3H), 0.83 (s, 3H), 0.79 (d, J = 7.4 Hz, 3H); ^{13}C NMR ($CDCl_3$, 150 MHz): δ 220.7, 193.0, 160.7, 150.3, 139.8, 110.7, 50.4, 48.6, 48.4, 46.3, 43.3, 42.2, 40.6, 39.8, 39.2, 39.1, 35.4, 35.2, 34.7, 31.5, 29.9, 21.8, 19.0, 18.0, 15.8; for NMR spectra see Supporting Information Figs. S10 and S11; HRMS (ESI) *m/z*: $[M+H]^+$ Calcd for $C_{25}H_{37}O_2$ 369.2788; Found 369.2772. The NMR data are in good agreement with the reported data[30].

*Variecolactone (**2**).* White powder; $[\alpha]_D^{25}$ +108.9 (*c* 0.5, CH_3CN); ^1H NMR ($CDCl_3$, 600 MHz): δ 6.96 (m, 1H), 4.71 (brd, J = 1.4 Hz, 1H), 4.63 (brs, 1H), 3.59 (m, 1H), 2.79 (m, 1H), 2.75 (m, 1H), 2.38 (td, J = 11.1, 5.6 Hz, 1H), 2.28−2.20 (m, 2H), 2.18−2.08 (m, 3H), 2.03−1.92 (m, 2H), 1.69 (brs, 3H), 1.54−1.40 (m, 5H), 1.36 (ddd, J = 13.7, 10.2, 5.6 Hz, 1H), 1.23 (q, J = 10.6 Hz, 1H), 1.08 (dd, J = 14.6, 1.4 Hz, 1H), 0.98 (dt, J = 13.7, 3.0 Hz, 1H), 0.90 (s, 3H), 0.86 (s, 3H), 0.68 (d, J = 7.2 Hz, 3H); ^{13}C NMR ($CDCl_3$, 150 MHz): δ 171.0, 150.5, 144.6, 125.3, 115.5, 110.4, 51.8, 48.1, 48.0, 44.8, 43.4, 40.8, 39.9, 39.8, 38.9, 38.6, 37.9, 35.1, 34.3, 30.0, 29.7, 21.7, 19.3, 18.1, 15.9; for NMR spectra see Figs. S12 and S13; HRMS (ESI) *m/z*: $[M+H]^+$ Calcd for $C_{25}H_{37}O_3$ 385.2737; Found 385.2728. The NMR data are in good agreement with the reported data[26].

*Emericolin A (**3**).* White powder; $[\alpha]_D^{23}$ +34.9 (*c* 0.26, $CHCl_3$); ^1H NMR ($CDCl_3$, 600 MHz): δ 9.29 (s, 1H), 6.76 (td, J = 5.3, 1.3 Hz, 1H), 4.75 (brd, J = 1.7 Hz, 1H), 4.65 (brs, 1H), 4.63 (m, 1H), 3.04 (m, 1H), 2.75 (m, 1H), 2.46−2.38 (m, 2H), 2.32−2.20 (m, 2H), 2.08−1.94 (m, 2H), 1.78 (td, J = 13.8, 4.6 Hz, 1H), 1.73 (m, 1H), 1.72 (brs, 1H), 1.52−1.35 (m, 5H), 1.27−1.20 (m, 2H), 1.14 (brd, J = 14.9 Hz, 1H), 0.97 (ddd, J = 14.0, 3.8, 2.5 Hz, 1H), 0.89 (s, 3H), 0.84 (s, 3H), 0.84 (d, J = 6.5 Hz, 3H); ^{13}C NMR ($CDCl_3$, 150 MHz): δ 199.5, 161.4, 150.5, 142.2, 110.5, 75.9, 52.8, 48.3, 48.1, 43.5, 41.2, 40.9, 40.3, 39.9, 38.5, 38.2, 37.7, 35.2, 34.2, 30.5, 29.8, 21.8, 19.0, 18.2, 15.4; for NMR spectra see Figs. S14 and S15; HRMS (ESI) *m/z*: $[M-H_2O+H]^+$ Calcd for $C_{25}H_{37}O$ 353.2839; Found 353.2831. The NMR data are in good agreement with the reported data[28].

*Variecoladiene (**4**).* Colorless oil; $[\alpha]_D^{22}$ +34.0 (*c* 0.93, $CHCl_3$); for NMR data and spectra see Supporting Information Table S7, Fig. S1, and Figs. S16−S21; HRMS (APCI) *m/z*: $[M + H]^+$ Calcd for $C_{25}H_{41}$ 341.3203; Found 341.3199.

*4α-Hydroxyvariecoladiene (**5**).* Colorless oil; $[\alpha]_D^{22}$ +21.1 (*c* 1.00, $CHCl_3$); for NMR data and spectra see Table S7, Fig. S1, and Supporting Information Figs. S22−S27; HRMS (ESI) *m/z*: $[M-H_2O+H]^+$ Calcd for $C_{25}H_{39}$ 339.3046; Found 339.3039.

*(23R)-Oxidovariecoladiene (**6**).* Colorless oil; $[\alpha]_D^{22}$ +47.0 (*c* 1.00, $CHCl_3$); for NMR data and spectra see Table S7, Fig. S1, and Supporting Information Figs. S30−S35; HRMS (APCI) *m/z*: $[M+H]^+$ Calcd for $C_{25}H_{41}O$ 357.3152; Found 357.3140.

*(23S)-Oxidovariecoladiene (**7**).* Colorless oil; $[\alpha]_D^{22}$ +51.9 (*c* 0.33, $CHCl_3$); for NMR data and spectra see Table S7, Fig. S1, and Supporting Information Figs. S36−S41; HRMS (APCI) *m/z*: $[M+H]^+$ Calcd for $C_{25}H_{41}O$ 357.3152; Found 357.3140.

4.15. X-ray crystallographic analysis

A single crystal of compound **7** was formed in DMSO by a slow evaporation process at room temperature for approximately three weeks. Single crystal X-ray diffraction measurements were performed on a Bruker D8 Venture diffractometer using Cu Kα radiation at 213 K. The data collection was performed with the APEX3 program, and cell refinement and data reduction were carried out using the SAINT program. The structure of **7** was solved by direct method with the SHELXT program and refined using the SHELXL program. All non-hydrogen atoms were refined anisotropically, whereas hydrogen atoms were placed by geometrical calculations. See the X-ray Crystallographic Data section in the Supporting Information for more details.

Acknowledgments

This work was performed for the iGEM 2021 Competition, and the financial support received from the Department of Chemistry, City University of Hong Kong, is greatly appreciated. We also thank Prof. Katsuya Gomi (Tohoku University) and Profs. Katsuhiko Kitamoto and Jun-ichi Maruyama (The University of Tokyo) for providing the expression vectors and the fungal strain. We are grateful to Dr. Man-Kit Tse (City University of Hong Kong) and Dr. Shek-Man Yiu (City University of Hong Kong) for their assistance with NMR spectra acquisition and X-ray diffraction data collection and analysis, respectively. This work was supported in part by an Early Career Scheme grant from the Research Grants Council (RGC) of Hong Kong (Project No. 21300219 (Y.M)). M.V.B acknowledges support from the City University of Hong Kong (Project No. 9610518).

Author contributions

Richard Y. C. Kong, Maria V. Babak, and Yudai Matsuda designed the research. Dexiu Yan, Teng Wan, and Tsz Ki Chan constructed the *A. oryzae* expression systems and isolated the metabolites. Jemma Arakelyan, Vladimir Kushnarev, and Nikolay S. Karnaukhov investigated the biological activities of the obtained compounds *in vitro* and *in vivo*. All authors analyzed the data and cowrote the manuscript.

Conflicts of interest

There are no conflicts to declare.

Appendix A. Supporting information

Supporting data to this article can be found online at https://doi.org/10.1016/j.apsb.2023.08.025.

References

1. Mitsuhashi T, Abe I. Sesterterpenoids. In: Kinghorn AD, Falk H, Gibbons S, Kobayashi Ji, Asakawa Y, Liu JK, editors. *Progress in the chemistry of organic natural products 111*. Cham: Springer International Publishing; 2020. p. 1−79.
2. Li K, Gustafson KR. Sesterterpenoids: chemistry, biology, and biosynthesis. *Nat Prod Rep* 2021;**38**:1251−81.
3. Zhang P, Qi J, Duan Y, Gao JM, Liu C. Research progress on fungal sesterterpenoids biosynthesis. *J Fungi* 2022;**8**:1080.
4. Masi M, Dasari R, Evidente A, Mathieu V, Kornienko A. Chemistry and biology of ophiobolin A and its congeners. *Bioorg Med Chem Lett* 2019;**29**:859−69.
5. Chiba R, Minami A, Gomi K, Oikawa H. Identification of ophiobolin F synthase by a genome mining approach: a sesterterpene synthase from *Aspergillus clavatus*. *Org Lett* 2013;**15**:594−7.
6. Matsuda Y, Mitsuhashi T, Quan Z, Abe I. Molecular basis for stellatic acid biosynthesis: a genome mining approach for discovery of sesterterpene synthases. *Org Lett* 2015;**17**:4644−7.
7. Narita K, Chiba R, Minami A, Kodama M, Fujii I, Gomi K, et al. Multiple oxidative modifications in the ophiobolin biosynthesis: P450 oxidations found in genome mining. *Org Lett* 2016;**18**:1980−3.
8. Huang JH, Lv JM, Wang QZ, Zou J, Lu YJ, Wang QL, et al. Biosynthesis of an anti-tuberculosis sesterterpenoid asperterpenoid A. *Org Biomol Chem* 2019;**17**:248−51.
9. Quan Z, Dickschat JS. Biosynthetic gene cluster for asperterpenols A and B and the cyclization mechanism of asperterpenol A synthase. *Org Lett* 2020;**22**:7552−5.
10. Ye Y, Minami A, Mandi A, Liu C, Taniguchi T, Kuzuyama T, et al. Genome mining for sesterterpenes using bifunctional terpene synthases reveals a unified intermediate of di/sesterterpenes. *J Am Chem Soc* 2015;**137**:11846−53.
11. Matsuda Y, Mitsuhashi T, Lee S, Hoshino M, Mori T, Okada M, et al. Astellifadiene: structure determination by NMR spectroscopy and crystalline sponge method, and elucidation of its biosynthesis. *Angew Chem Int Ed* 2016;**55**:5785−8.
12. Okada M, Matsuda Y, Mitsuhashi T, Hoshino S, Mori T, Nakagawa K, et al. Genome-based discovery of an unprecedented cyclization mode in fungal sesterterpenoid biosynthesis. *J Am Chem Soc* 2016;**138**:10011−8.

13. Mitsuhashi T, Rinkel J, Okada M, Abe I, Dickschat JS. Mechanistic characterization of two chimeric sesterterpene synthases from *Penicillium*. *Chem Eur J* 2017;**23**:10053−7.
14. Narita K, Sato H, Minami A, Kudo K, Gao L, Liu C, et al. Focused genome mining of structurally related sesterterpenes: enzymatic formation of enantiomeric and diastereomeric products. *Org Lett* 2017;**19**:6696−9.
15. Gao L, Narita K, Ozaki T, Kumakura N, Gan P, Minami A, et al. Identification of novel sesterterpenes by genome mining of phytopathogenic fungi *Phoma* and *Colletotrichum* sp. *Tetrahedron Lett* 2018;**59**:1136−9.
16. Guo J, Cai Y-S, Cheng F, Yang C, Zhang W, Yu W, et al. Genome mining reveals a multiproduct sesterterpenoid biosynthetic gene cluster in *Aspergillus ustus*. *Org Lett* 2021;**23**:1525−9.
17. Jiang L, Zhang X, Sato Y, Zhu G, Minami A, Zhang W, et al. Genome-based discovery of enantiomeric pentacyclic sesterterpenes catalyzed by fungal bifunctional terpene synthases. *Org Lett* 2021;**23**:4645−50.
18. Chen R, Jia Q, Mu X, Hu B, Sun X, Deng Z, et al. Systematic mining of fungal chimeric terpene synthases using an efficient precursor-providing yeast chassis. *Proc Natl Acad Sci U S A* 2021;**118**:e2023247118.
19. Jiang L, Zhu G, Han J, Hou C, Zhang X, Wang Z, et al. Genome-guided investigation of anti-inflammatory sesterterpenoids with 5−15 *trans*-fused ring system from phytopathogenic fungi. *Appl Microbiol Biotechnol* 2021;**105**:5407−17.
20. Jiang L, Yang H, Zhang X, Li X, Lv K, Zhang W, et al. Schultriene and nigtetraene: two sesterterpenes characterized from pathogenetic fungi via genome mining approach. *Appl Microbiol Biotechnol* 2022;**106**:6047−57.
21. Qiao Y, Xu Q, Huang Z, Chen X, Ren X, Yuan W, et al. Genome mining reveals a new cyclopentane-forming sesterterpene synthase with unprecedented stereo-control. *Org Chem Front* 2022;**9**:5808−18.
22. Li D, Yang M, Mu R, Luo S, Chen Y, Li W, et al. Characterization of two chimeric sesterterpene synthases from a fungal symbiont isolated from a sesterterpenoid-producing Lamiaceae plant *Leucosceptrum canum*. *Chin Chem Lett* 2023;**34**:107469.
23. Christianson DW. Structural and chemical biology of terpenoid cyclases. *Chem Rev* 2017;**117**:11570−648.
24. Hensens OD, Zink D, Williamson JM, Lotti VJ, Chang RS, Goetz MA. Variecolin, a sesterterpenoid of novel skeleton from *Aspergillus variecolor* MF138. *J Org Chem* 1991;**56**:3399−403.
25. Tezuka Y, Takahashi A, Maruyama M, Tamamura T, Kutsuma S, Naganawa H, et al., Inventors. Novel antibiotics, AB5362-A, B, and C, their manufacture, their use as fungicides, and Phoma species AB5362. US patent 100456621998.
26. Takahashi H, Hosoe T, Nozawa K, Kawai KI. Two new sesterterpenes from the ascomycetous fungus *Emericella purpurea*. *J Nat Prod* 1999;**62**:1712−3.
27. Fujimoto H, Nakamura E, Okuyama E, Ishibashi M. Immunomodulatory constituents from an ascomycete, *Emericella aurantio-brunnea*. *Chem Pharm Bull* 2000;**48**:1436−41.
28. Yoganathan K, Rossant C, Glover RP, Cao S, Vittal JJ, Ng S, et al. Inhibition of the human chemokine receptor CCR5 by variecolin and variecolol and isolation of four new variecolin analogues, emericolins A−D, from *Emericella aurantiobrunnea*. *J Nat Prod* 2004;**67**:1681−4.
29. Joudaa JB, Fopossib JLD, Mbazoaa CD, Wandjia J. Antibacterial activity of the major compound of an endophytic fungus isolated from *Garcinia preussii*. *J Appl Pharm Sci* 2016:26−9.
30. Yodsing N, Lekphrom R, Sangsopha W, Aimi T, Boonlue S. Secondary metabolites and their biological activity from *Aspergillus aculeatus* KKU-CT2. *Curr Microbiol* 2018;**75**:513−8.
31. Piers E, Boulet SL. Total syntheses of the diterpenoids (±)-verrucosan-2β-ol, (±)-neoverrucosan-5β-ol, and (±)-homoverrucosan-5β-ol. An approach to the synthesis of the sesterterpenoid variecolin. *Tetrahedron Lett* 1997;**38**:8815−8.
32. Molander GA, Quirmbach MS, Silva LF, Spencer KC, Balsells J. Toward the total synthesis of variecolin. *Org Lett* 2001;**3**:2257−60.
33. Li K, Wang C, Yin G, Gao S. Construction of the basic skeleton of ophiobolin A and variecolin. *Org Biomol Chem* 2013;**11**:7550−8.
34. Krout MR, Henry CE, Jensen T, Wu KL, Virgil SC, Stoltz BM. Wolff/Cope approach to the AB ring of the sesterterpenoid variecolin. *J Org Chem* 2018;**83**:6995−7009.
35. de Vries RP, Riley R, Wiebenga A, Aguilar-Osorio G, Amillis S, Uchima CA, et al. Comparative genomics reveals high biological diversity and specific adaptations in the industrially and medically important fungal genus *Aspergillus*. *Genome Biol* 2017;**18**:28.
36. Jouda JB, Fopossi JLD, Kengne FM, Djama Mbazoa C, Golz C, Strohmann C, et al. Secondary metabolites from *Aspergillus japonicus* CAM231, an endophytic fungus associated with *Garcinia preussii*. *Nat Prod Res* 2017;**31**:861−9.
37. Jin FJ, Maruyama J, Juvvadi PR, Arioka M, Kitamoto K. Development of a novel quadruple auxotrophic host transformation system by *argB* gene disruption using *adeA* gene and exploiting adenine auxotrophy in *Aspergillus oryzae*. *FEMS Microbiol Lett* 2004;**239**:79−85.
38. Takino J, Kozaki T, Sato Y, Liu C, Ozaki T, Minami A, et al. Unveiling biosynthesis of the phytohormone abscisic acid in fungi: unprecedented mechanism of core scaffold formation catalyzed by an unusual sesquiterpene synthase. *J Am Chem Soc* 2018;**140**:12392−5.
39. Tsukada K, Shinki S, Kaneko A, Murakami K, Irie K, Murai M, et al. Synthetic biology based construction of biological activity-related library of fungal decalin-containing diterpenoid pyrones. *Nat Commun* 2020;**11**:1830.
40. Kahlert L, Bassiony EF, Cox RJ, Skellam EJ. Diels−Alder reactions during the biosynthesis of sorbicillinoids. *Angew Chem Int Ed* 2020;**59**:5816−22.
41. Kahlert L, Villanueva M, Cox RJ, Skellam EJ. Biosynthesis of 6-hydroxymellein requires a collaborating polyketide synthase-like enzyme. *Angew Chem Int Ed* 2021;**60**:11423−9.
42. Tang J, Matsuda Y. Discovery of branching meroterpenoid biosynthetic pathways in *Aspergillus insuetus*: involvement of two terpene cyclases with distinct cyclization modes. *Chem Sci* 2022;**13**:10361−9.
43. Chen L, Wei X, Matsuda Y. Depside bond formation by the starter-unit acyltransferase domain of a fungal polyketide synthase. *J Am Chem Soc* 2022;**144**:19225−30.
44. Vesth TC, Nybo JL, Theobald S, Frisvad JC, Larsen TO, Nielsen KF, et al. Investigation of inter- and intraspecies variation through genome sequencing of *Aspergillus* section Nigri. *Nat Genet* 2018;**50**:1688−95.
45. Ohtani I, Kusumi T, Kashman Y, Kakisawa H. High-field FT NMR application of Mosher's method. The absolute configurations of marine terpenoids. *J Am Chem Soc* 1991;**113**:4092−6.
46. Duarte D, Nunes M, Ricardo S, Vale N. Combination of antimalarial and CNS drugs with antineoplastic agents in MCF-7 breast and HT-29 colon cancer cells: biosafety evaluation and mechanism of action. *Biomolecules* 2022;**12**:1490.
47. Savić MP, Djurendić EA, Petri ET, Ćelić A, Klisurić OR, Sakač MN, et al. Synthesis, structural analysis and antiproliferative activity of some novel D-homo lactone androstane derivatives. *RSC Adv* 2013;**3**:10385−95.
48. Marupudi NI, Han JE, Li KW, Renard VM, Tyler BM, Brem H. Paclitaxel: a review of adverse toxicities and novel delivery strategies. *Expet Opin Drug Saf* 2007;**6**:609−21.
49. Danúbia Silva dos S, Regina Coeli dos Santos G. Doxorubicin-induced cardiotoxicity: from mechanisms to development of efficient therapy. In: Wenyong T, editor. *Cardiotoxicity*. Rijeka: IntechOpen; 2018. Ch. 1.
50. Fujii T, Yamaoka H, Gomi K, Kitamoto K, Kumagai C. Cloning and nucleotide sequence of the ribonuclease T1 gene (*rntA*) from

Aspergillus oryzae and its expression in *Saccharomyces cerevisiae* and *Aspergillus oryzae*. *Biosci Biotechnol Biochem* 1995;**59**: 1869−74.
51. Jin F, Maruyama J, Juvvadi P, Arioka M, Kitamoto K. Adenine auxotrophic mutants of *Aspergillus oryzae*: development of a novel transformation system with triple auxotrophic hosts. *Biosci Biotechnol Biochem* 2004;**68**:656−62.
52. Wei X, Matsuyama T, Sato H, Yan D, Chan PM, Miyamoto K, et al. Molecular and computational bases for spirofuranone formation in setosusin biosynthesis. *J Am Chem Soc* 2021;**143**:17708−15.
53. Matsuda Y, Bai T, Phippen CBW, Nødvig CS, Kjærbølling I, Vesth TC, et al. Novofumigatonin biosynthesis involves a non-heme iron-dependent endoperoxide isomerase for orthoester formation. *Nat Commun* 2018;**9**:2587.
54. Fischer AH, Jacobson KA, Rose J, Zeller R. Hematoxylin and eosin staining of tissue and cell sections. *Cold Spring Harb Protoc* 2008; **2008**. pdb.prot4986.
55. Greaves P. Chapter 8−digestive system. In: Greaves P, editor. *Histopathology of preclinical toxicity studies*. 4th ed. Boston: Academic Press; 2012. p. 325−431.